Unveiling shrouded oceans on temperate sub-Neptunes via transit signatures of solubility equilibria vs. gas thermochemistry

Renyu Hu (renyu.hu@jpl.nasa.gov)
Jet Propulsion Lab https://orcid.org/0000-0003-2215-8485
Mario Damiano
Jet Propulsion Laboratory https://orcid.org/0000-0002-1830-8260
Markus Scheucher
Jet Propulsion Laboratory
Edwin Kite
University of Chicago https://orcid.org/0000-0002-1426-1186
Sara Seager
Massachusetts Institute of Technology https://orcid.org/0000-0002-6892-6948
Heike Rauer
DLR, German Aerospace Center

Research Article

Keywords: exoplanets, oceans, gas thermochemistry

Posted Date: May 11th, 2021

DOI: https://doi.org/10.21203/rs.3.rs-481864/v1

Unveiling shrouded oceans on temperate sub-Neptunes via transit signatures of solubility equilibria vs. gas thermochemistry

Renyu Hu[1,2], Mario Damiano[1], Markus Scheucher[1,3], Edwin Kite[4], Sara Seager[5,6,7], Heike Rauer[3,8]

[1]*Jet Propulsion Laboratory, California Institute of Technology, Pasadena, CA 91109, USA*

[2]*Division of Geological and Planetary Sciences, California Institute of Technology, Pasadena, CA 91125, USA*

[3]*Institut für Planetenforschung, Deutsches Zentrum für Luft- und Raumfahrt, D-12489 Berlin, Germany*

[4]*Department of the Geophysical Sciences, University of Chicago, Chicago, IL 60637, USA*

[5]*Department of Earth, Atmospheric, and Planetary Sciences, Massachusetts Institute of Technology, Cambridge, MA 02139, USA*

[6]*Department of Physics and Kavli Institute for Astrophysics and Space Research, Massachusetts Institute of Technology, Cambridge, MA 02139, USA*

[7]*Department of Aeronautics and Astronautics, Massachusetts Institute of Technology, Cambridge, MA 02139, USA*

[8]*Institut für Geologische Wissenschaften, Freie Universität Berlin, D-12249 Berlin, Germany*

The recent discovery and initial characterization of sub-Neptune-sized exoplanets that receive stellar irradiance of approximately Earth's[1–7] raised the prospect of finding habitable planets in the coming decade. Some of these temperate planets may support liquid water oceans, if they do not have massive H_2/He envelopes and are thus not too hot at the bottom of the envelopes[8–11]. For planets larger than Earth, and especially planets in the $1.7 - 3.5\ R_\oplus$ population[12], the mass of the H_2/He envelope is typically not sufficiently constrained to assess the potential habitability[13–16]. Here we show that the solubility equilibria vs. thermochemistry of carbon and nitrogen gases results in observable discriminators between small H_2 atmospheres vs. massive ones. On temperate sub-Neptunes, the condition to form a liquid-water ocean and that to achieve the thermochemical equilibrium are mutually exclusive. The dominant carbon and nitrogen gases are typically CH_4 and NH_3 due to thermochemical recycling in a massive atmosphere of a temperate

planet, and those in a small atmosphere overlying a liquid-water ocean are most likely CO_2 and N_2, followed by CO and CH_4 produced photochemically. NH_3 is depleted in the small atmosphere by dissolution into the liquid-water ocean[17]. These gases lead to distinctive features in the planet's transmission spectrum, and a moderate number of repeated transit observations with the James Webb Space Telescope should readily tell apart a small atmosphere vs. a massive one via these spectral features on planets like K2-18 b. This method thus provides a way to use near-term facilities to constrain the atmospheric mass and habitability of temperate sub-Neptune exoplanets.

The exoplanet community already has ways to detect an H_2 atmosphere by transmission spectroscopy via its pressure scale height one order of magnitude larger than that of an N_2 or CO_2 atmosphere[18]. However, the mass of the H_2 atmosphere – the parameter that controls the temperature at the bottom of the atmosphere and thus the possibility for liquid water[8–10] – is not directly measurable from the transmission spectrum. Also, a planet's mass and radius typically allow multiple models of the interior structure[13,14]. It is unclear whether the planets in the $1.7-3.5\ R_\oplus$ population are mostly rocky planets with massive H_2/He gas envelopes[19,20] or planets with a massive water layer (~ 50 wt. %) that do not require a large H_2 envelope to explain their radius[15,16,21]. Direct-imaging observations in the future may provide means to detect a surface underneath a thin atmosphere on temperate planets, via the ocean glint[22] or surface heterogeneity[23,24]. However, these methods are not applicable to the near-term capabilities such as the JWST and may pose challenges on precision even for direct-imaging mission concepts[25]. Here we propose that transit observations of temperature sub-Neptunes in the near- and mid-infrared wavelengths, which will soon commence, can detect small H_2 atmospheres that support liquid-water oceans and distinguish them from massive atmospheres.

The temperate sub-Neptune K2-18 b is a harbinger of a class of planets that might be habitable and exemplifies the need for a near-term method to measure the size of an H_2 atmosphere. The planet of $8.6\ M_\oplus$ and $2.6\ R_\oplus$ is in the habitable zone of an M dwarf star, and has a transmission spectrum (obtained by *Hubble* at $1.1-1.7\ \mu m$) with confirmed spectral features, which indicates that the planet should host an atmosphere dominated by H_2[6,7].

Interior structure models showed that the planet can have a massive ($>\sim 1000$ bar) H_2 atmosphere overlaying a rocky/Fe core and a supercritical water layer, or a smaller (< 100 bar) H_2 atmosphere with a water-dominated interior[11,16]. For K2-18 b, specifically, a $\sim 10 - 100$ bar H_2 atmosphere overlaying a water layer would cause > 200 bar of water to evaporate into the atmosphere, resulting in a hot steam atmosphere inconsistent with the observed transmission spectrum[26]. An even smaller, ~ 1 bar H_2 atmosphere would prevent this steam atmosphere and produce a liquid-water ocean (see Methods), but requires a very small rocky/Fe core and may be disfavored from the planet formation standpoint[27]. However, a planet slightly more massive or smaller than K2-18 b – such as those at the center of the $1.7 - 3.5\ R_\oplus$ planet population[15] – does not have this small-core difficulty to have a small atmosphere, and many such planets and planet candidates have been detected and will soon be available for transmission spectroscopy (Fig. 1).

How can we distinguish a planet with a massive H_2 atmosphere versus an ocean planet with a small H_2 atmosphere? Here we propose, for temperate planets, these two scenarios can be distinguished by detecting signature gases of the gas-phase thermochemical equilibrium vs. solubility equilibria. The key difference between the two scenarios is that the gas-phase thermochemical equilibrium would be achieved in the deep and hot part of the massive atmosphere, and in contrast, it would not be achieved in a small atmosphere overlying a liquid-water ocean. Instead, NH_3 and sulfur species would be sequestered by the ocean[17,28] and the abundance of CO_2 would be set by the ocean chemistry (Fig. 2, with the cosmochemical and geological constraints detailed in Methods). This fundamental difference, coupled with photochemical processes, leads to distinctive gas abundances in the observable part ($<\sim 0.1$ bar) of the atmosphere.

If the planet has a massive H_2 atmosphere, thermochemical reactions in the deep atmosphere recycle O, C, N, S species into H_2O, CH_4, NH_3, and H_2S[29–32]. H_2O can form a cloud and the above-cloud H_2O may be partially depleted as a result[33–35]. Recent calculations have shown that the photodissociation of NH_3 in the presence of CH_4 leads to the formation of HCN, and that CO and CO_2 are produced by the photodissociation of CH_4 together with H_2O[35]. The photodissociation of H_2S leads to the formation of elemental sulfur haze[36,37], but the haze would

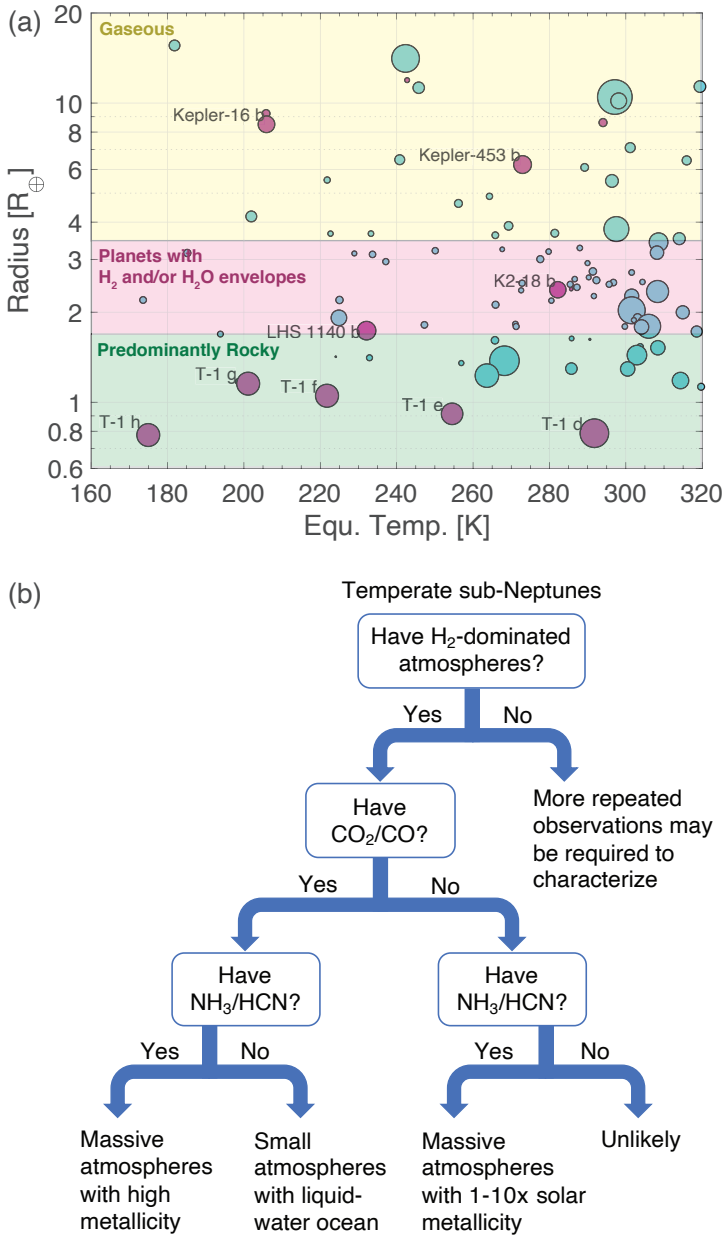

Figure 1: Temperate exoplanets amenable for atmospheric characterization via transmission spectroscopy. (a) Purple dots are confirmed planets with measured masses, and blue dots are planets with unknown masses or planet candidates. Data are taken from the NASA Exoplanet Archive and and the TESS Objects of Interest Catalog. The marker sizes are scaled with the expected S/N of the spectral features of an H_2 atmosphere observed by JWST at 2 μm. Most of the temperate planets and planet candidates suitable for atmospheric characterization are larger than Earth and thus more likely to have H_2 atmospheres. (b) A roadmap to characterize the mass of the atmospheres and the habitability of temperate sub-Neptunes by detecting signature gases. See text for details.

be close to the cloud deck and would not mute transmission spectral features[35]. These photochemical products are transported to the deep atmosphere and recycled back to CH_4, NH_3, and H_2S. An exception is the $100\times$ solar metallicity atmosphere, where the thermochemical-equilibrium mixing ratios of N_2 and NH_3 may be similar and those of CO and CO_2 can be substantial compared with the mixing ratios produced by the photodissociation of CH_4 and H_2O (see Methods).

If the planet instead has a small atmosphere and a liquid-water ocean, this thermochemical recycling cannot occur. Instead, CO_2 is the preferred form of carbon in equilibrium with a massive amount of H_2O[32,38], and NH_3 is dissolved in the ocean and largely depleted from the atmosphere[17]. The abundance of atmospheric CO_2 is controlled by the oceanic pH[39–42] and that of N_2 is probably a combined result of the initial endowment and atmospheric escape. A reasonable lower bound of the total mass of CO_2 in the H_2 and H_2O layers (Fig. 2) can be derived from the cosmochemical constraints of planetary building blocks and the partitioning between the iron core, the silicate mantle, and the water layer (see Methods). Also, the "seafloor" of this thin-atmosphere, H_2O-rich sub-Neptune will not be not a sharp interface in density and composition, but instead have a finite thickness[43]. The interface will be compositionally stratified with denser material underlying less dense material, and material transport across this "fuzzy layer" is inhibited due to the stratification. Thus, any carbon or nitrogen added to the H_2 and H_2O envelope by planetesimal accretion late in planet growth will remain in the envelope, and will not be stirred down into the silicate layer. Meanwhile, transit observations can straightforwardly identify H_2-dominated atmospheres and rule out CO_2 or N_2-dominated ones only from the size of spectral features[18].

We have used an atmospheric photochemical model[44] coupled with a radiative-convective model[26] to determine the equilibrium abundances of CO, CH_4, and C_2H_6 in small and temperate H_2 atmospheres, for a cosmochemically and geologically plausible range of CO_2 abundance, and compared the compositions and transmission spectra with massive H_2 atmospheres[35]. The input parameters and atmospheric chemistry results of the small-atmosphere models are summarized in Methods. We have used the planetary parameters of K2-18 b[7,45] and the UV spectrum of the M dwarf star GJ 176[46] (similar to K2-18[47]) in these models, even though K2-18 b probably

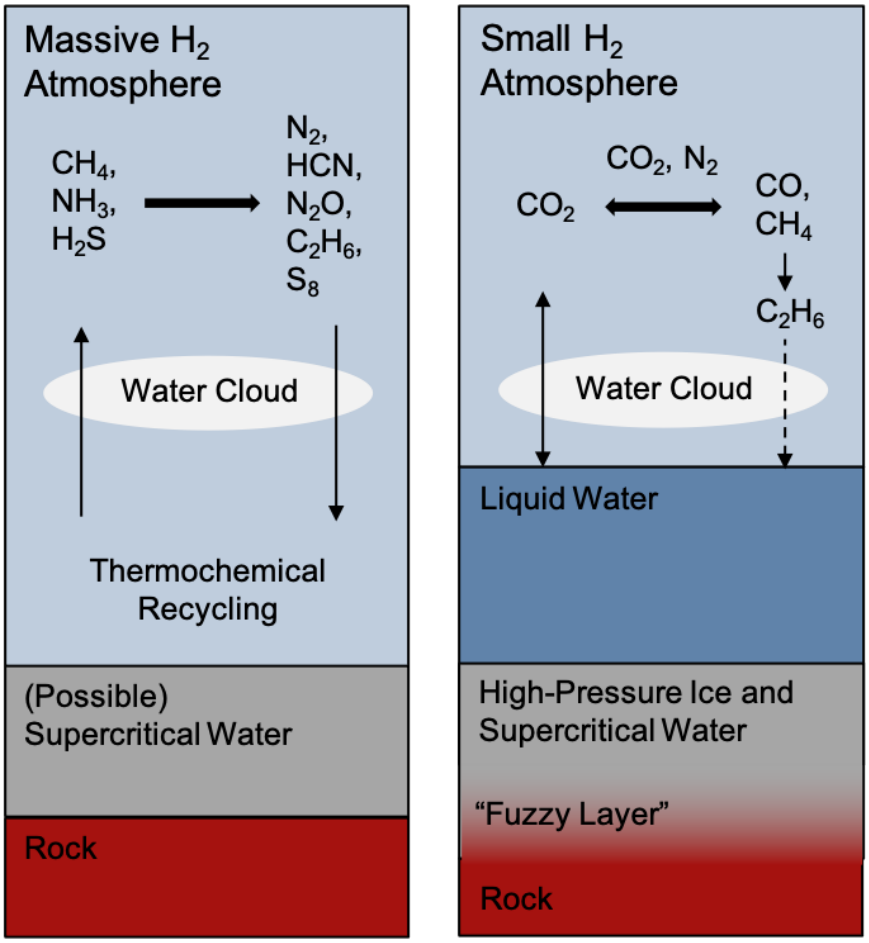

Figure 2: Interior structures of temperate H-rich exoplanets and the associated ranges of atmospheric composition. If the planet has a massive H_2 atmosphere, the deep atmosphere would be hot – enabling thermochemical recycling – but a liquid-water surface would not be possible. If the planet has a small H_2 atmosphere, a liquid-water surface may be possible. On these planets, the equilibrium abundance of atmospheric CO_2 is set by the oceanic chemistry and that of N_2 by atmospheric evolution.

does not have a small atmosphere. The results should be broadly applicable to temperate sub-Neptunes around M dwarf stars, because the differences in atmospheric composition and transmission spectrum are driven by gas-phase thermochemical equilibrium vs. solubility equilibria, and not by basic planetary parameters such as surface gravity. Fig. 3 compares the expected spectra for the massive-atmosphere scenarios and the small-atmosphere scenarios. For K2-18 b, both the massive-atmosphere models with $1 - 100\times$ solar metallicity and the small-atmosphere models with a low mixing ratio of CO_2 (400 ppm) provide good fits to the transmission spectrum measured by *Hubble*.

Measuring the transmission spectra in an expanded wavelength range of $1 - 5$ μm will distinguish the small atmospheres from massive ones. Using K2-18 b as an example for temperate sub-Neptunes, we see that the massive-atmosphere models and the small-atmosphere models, while having differences within each group, can be distinguished using the spectral regions of $1.7 - 2.1$, $2.6 - 3.1$, and $4.1 - 4.9$ μm (the shaded areas in Fig. 3). Both the massive-atmosphere and small-atmosphere models show spectral features of H_2O and CH_4, and so observing these two gases alone is unlikely to separate the scenarios. At $1.7 - 2.1$ and $2.6 - 3.1$ μm, the transmission spectra show NH_3 and HCN absorption in massive atmospheres but not in small atmospheres. At ~ 2.8 μm, the transmission spectra of small atmospheres show CO_2 absorption. Between 4.1 and 4.9 μm, the transmission spectra of small atmospheres (the low-CO_2 cases) have prominent features of CO_2 and CO, and these features are much weaker in the spectra of massive atmospheres.

The massive atmosphere with $100\times$ solar metallicity can have CO and CO_2 produced from CH_4 and H_2O photolysis[35], and also from gas-phase thermochemical equilibrium (see Methods). The mixing ratios of CO and CO_2 can be comparable with the small atmosphere models. Will these effects create a "false positive" where a massive atmosphere might be mistaken as a small atmosphere, since they could have similar mixing ratios of CO and CO_2 at the ~ 0.1 bar level? Fig. 3 indicates that this mistake will be unlikely, because (1) the spectrum of the massive atmosphere also features NH_3 and HCN absorption but the small atmosphere spectrum does not; (2) the massive atmosphere with $100\times$ solar metallicity has a greater mean molecular weight (~ 5) than the small

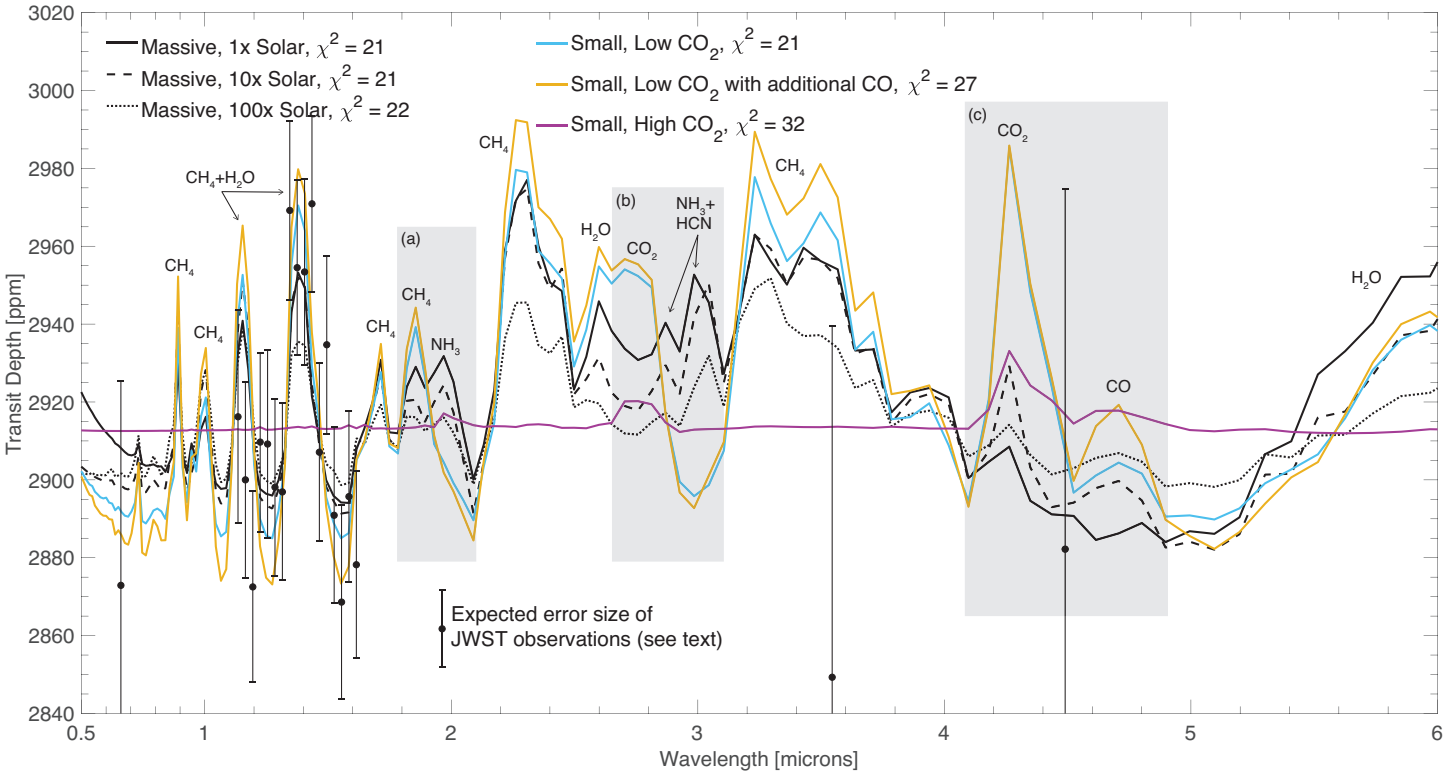

Figure 3: Expected transmission spectrum of temperate sub-Neptune planets of M dwarf stars, using K2-18 b as an example and comparing with the planet's transit depth observed by K2, *Hubble* and *Spitzer*[7]. The massive-H_2-atmosphere models and the small-H_2-atmosphere models differ in three spectral regions: in (a) and (b), the massive-atmosphere models have absorption features of NH_3 and HCN, while the small-atmosphere models do not; in (c), the small-atmosphere models with a low mixing ratio of CO_2 (400 ppm) have prominent features of CO_2 and CO, while the massive-atmosphere models only have small features of CO_2. The small-atmosphere models with a high mixing ratio of CO_2 (10%) has a high mean molecular weight (~ 7) and a cloud top at $\sim 10^{-3}$ bar (as opposed to $\sim 3 \times 10^{-2}$ bar the low-CO_2 cases) and thus muted spectral features.

atmosphere (~ 2 in the low-CO_2 cases) and thus smaller transmission features; and (3) the massive atmosphere will have $CO_2/CO < \sim 0.1$[35], and the small atmosphere typically has $CO_2/CO > 1$ (Table 1). Furthermore, a massive atmosphere with $\gg 100\times$ solar metallicity will have a mean molecular weight much higher than that of an H_2 atmosphere and is thus also distinguishable by transmission spectroscopy.

With moderate time investment (i.e.,< 100 hours), JWST will provide the sensitivity to detect the signature gases aforementioned and distinguish massive versus small atmospheres on planets like K2-18 b. As an example, we have used PandExo[48] to simulate the expected photometric precision using JWST's NIRSpec instrument. If combining two transit observations with NIRSpec's G235H grating and four transits with the G395H grating, the overall photometric precision would be ~ 20 ppm per spectral element at a resolution of $R = 100$ in both channels that cover a wavelength range of 1.7 – 5.2 μm. These observations would distinguish the small-atmosphere scenarios versus the massive-atmosphere scenarios at $> 4.5\sigma$. Additionally, spectral retrievals using Tau-REx[49] indicate that the abundance of NH_3 and HCN in massive atmospheres and that of CO_2 and CO in small atmospheres would be usefully constrained (Fig. S1). The dedicated exoplanet atmosphere characterization mission ARIEL could also provide the senstivity to detect these gases with more repeated transit observations[50].

Taken together, the results presented here identify a near-term path to detect small H_2 atmospheres that can be consistent with liquid-water oceans on temperate exoplanets. H_2 atmospheres are probably the only type of temperate atmospheres readily within the reach of JWST and ARIEL for detailed studies, since to characterize a heavier N_2 or CO_2 atmosphere will require co-adding a few tens transits – something not impossible but probably very hard[51–55]. The mass of the H_2 atmospheres – a parameter that is not directly measured by transits but critical for habitability – can be inferred from transmission spectra via the signature gases that indicate solubility equilibria versus gas-phase thermochemical recycling. The biggest uncertainty is probably the temperature at the ~ 100-bar pressure level in the massive-atmosphere scenarios, which may be affected by ad hot heating mechanisms such as tidal heating. Detailed models of the interior temperature and mixing may further constrain this uncertainty[56]. Based on the considerable range of the parameter space explored, we suggest that the sensitivity of multiple gases

provided by future observatories' expanded wavelength coverage over *Hubble* would enable broad categorization of small versus massive atmospheres, as summarized in Fig. 1. If some of the temperate planets and planet candidates have small H_2 atmospheres, their relative ease for transit observations would significantly enhance the prospect of detecting and characterizing potentially habitable exoplanets within the next decade.

Methods

Mutual exclusivity of habitability and thermochemical equilibrium On temperate sub-Neptunes, the condition to form a liquid-water ocean and that to achieve the thermochemical equilibrium of carbon and nitrogen molecules are mutually exclusive. The conversion rate between CO/CO_2 and CH_4, and that between N_2 and NH_3, are primarily a function of the temperature and to a lesser extent the pressure[57,58]. To effectively recycle a molecule, its chemical lifetime must be shorter than the vertical mixing timescale. The vertical mixing timescale, in turn, is related to the internal heat flux of the planet in the convective layer of the atmosphere[59]. To have a chemical lifetime of CO that equals to or is shorter than the vertical mixing timescale, the temperature is typically > 1000 K. N_2 is expected to reach thermochemical equilibrium at even higher temperatures.

Fig. 4 shows the "quench point" of carbon and nitrogen species on a temperate sub-Neptune like K2-18 b with massive H_2 atmospheres, based on the pressure-temperature profiles adopted in the massive-atmosphere models[35]. The "quench point" is defined as the pressure level where the chemical lifetime of a gas equals to the vertical mixing timescale[57,58]. The gas is close to thermochemical equilibrium at or below the quench point, and its mixing ratio is carried to the atmosphere above the quench point by vertical mixing. On temperate sub-Neptunes, carbon species should reach thermochemical equilibrium at the temperature of $1000 - 1200$ K and the pressure of > 100 bar. Nitrogen species reach thermochemical equilibrium at the higher temperature of ~ 1400 K. These temperatures are substantially higher than the critical point of water. As such, we do not expect thermochemical equilibrium of carbon and nitrogen molecules on a temperate planet with a liquid-water ocean. Conversely, a temperate planet with a massive H_2 atmosphere that achieves thermochemical equilibrium at depths

is not habitable.

One might also consider the intermediate situation between massive atmospheres with thermochemical equilibrium and small atmospheres with liquid-water oceans, e.g., the atmospheres with a surface pressure of 1 – 100 bars (Fig. 4). For many sub-Neptunes, this intermediate-atmosphere scenario would still require a massive water layer underneath to explain their mass and radius. If water is in the liquid form at the interface with the atmosphere, the evaporation of this ocean will make the atmosphere H_2O-dominated[26]. If water is supercritical, any H_2 layer of 1 – 100 bars should be well mixed with the water layer. Therefore, such an intermediate endowment of H_2 would most likely result in a non-H_2-dominated atmosphere, which is distinguishable with transmission spectroscopy[18].

Massive atmosphere models. The photochemical models of massive, H_2-dominated atmospheres are described in a companion paper[35]. In this work, we adopt the massive atmosphere models of K2-18 b and compare them with the small atmosphere models. The massive atmosphere models explore the atmospheric metallicity of $1 - 100\times$ solar abundance.

The photochemical models of the massive atmospheres assume that the dominant O, C, N, and S species are H_2O, CH_4, NH_3, and H_2S at the base of the photochemical domain, which was defined as the pressure level 10-fold greater than the tropopause pressure (i.e., typically around 1 bar)[35]. Gases produced in the modeled domain can be transported through the lower boundary. This setup assumes that thermochemical recycling in the deeper atmosphere effectively recycles the photochemical products into H_2O, CH_4, NH_3, and H_2S. Here, based on the quench points shown in Fig. 4, we can further assess how realistic this assumption is. Fig. 4 shows that, at the quench point of CO–CH_4, the temperature is likely deep in the CH_4-dominated regime. The same is also true for the N_2–NH_3, except for the $100\times$ solar-metallicity case in which the quench point is close to the equal-abundance boundary between N_2 and NH_3. A quantitative description of this behavior is provided below. Note that the quench point depends on the strength of vertical mixing and the deep-atmosphere temperature depends on the thermal history of the planet, and so the detail behavior may be complex[56].

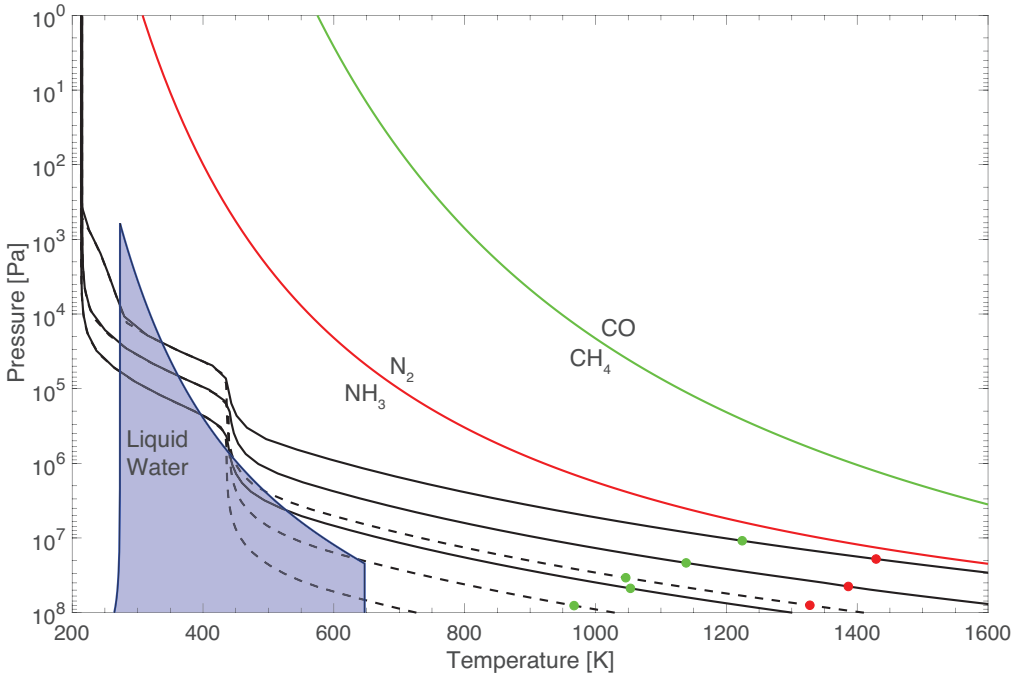

Figure 4: Modeled pressure-temperature profiles of a sub-Neptune exoplanet like K2-18 b with massive H_2 atmospheres that receive stellar irradiance of Earth's, for an internal heat flux of $T_{\rm int} = 60$ K (similar to Neptune, black solid lines) and $T_{\rm int} = 30$ K (similar to Earth, black dashed lines). The pressure-temperature profiles assume $1\times$, $10\times$, and $100\times$ solar metallicity. The shaded area shows the pressure and temperature range where pure liquid water is stable. The green and red lines show the equal-abundance boundaries for major carbon and nitrogen gases in a solar-metallicity gas in thermochemical equilibrium, and the green and red dots show the expected quench point for CO and that for N_2 respectively. The quench points are estimated by equating the chemical lifetime to the vertical mixing timescale[57,58,60], with the eddy diffusion coefficient estimated using a mixing-length theory[59] ($\sim 10^4$ m^2 s^{-1} at the pressure of $10^6 - 10^8$ Pa). The quench point for CO_2 follows that of CO, and similarly, that of HCN occurs at a similar pressure and temperature as N_2[57,58].

Applying a thermochemical equilibrium model[38], we find that for $1-10\times$ solar metallicity and at the quench pressure, the mixing ratio of CO is $10^{-10} - 10^{-8}$ and that of CO_2 is $< 10^{-10}$. These quantities are substantially smaller than the respective mixing ratios found by the photochemical models at the lower boundary. The mixing ratio of N_2 is $10^{-6} - 10^{-4}$, and that of HCN is minimal. These estimates indicate that the $1 - 10\times$ solar massive atmospheres on temperate planets are safely in the CH_4- and NH_3-dominated regime, and the assumption that the dominant C and N species are CH_4 and NH_3 at the base of the photochemical domain is valid.

For the $100\times$ solar metallicity case, the mixing ratios of CO at the quench pressure can reach $10^{-5}-10^{-2}$ and that of CO_2 can reach $10^{-6} - 10^{-3}$, with the pressure-temperature profiles shown in Fig. 4, which can exceed the mixing ratios found by the photochemical model at ~ 1 bar level[35]. While CH_4 is still the dominant carbon-bearing molecule, a higher deep-atmosphere temperature would result in greater mixing ratios of CO and CO_2. This comparison indicates that the mixing ratio of CO and CO_2 in the part of the atmosphere probed by transmission spectroscopy (typically $10^2 - 10^4$ Pa) can indeed reach or exceed the $10^{-6} - 10^{-2}$ level. The mixing ratio of N_2 at the quench pressure is comparable to that of NH_3 and that of HCN is $\sim 10^{-6}$. Again, a higher deep-atmosphere temperature favors N_2 and further reduces the equilibrium abundance of NH_3. The input mixing ratio of NH_3 in the photochemical model for the $100\times$ solar massive atmosphere may thus be overestimated, while the photochemical production of HCN should still dominate in the observable part of the atmosphere. Because the mixing ratio of NH_3 expected in small atmospheres is $< 10^{-12}$ (Fig. 6), and because the spectral features of NH_3 and HCN are already prominent at the $10^{-6} - 10^{-4}$ level[35], even reducing the mixing ratio of NH_3 in the massive atmosphere by a few orders of magnitude would not make its transmission spectrum similar to that of a small atmosphere. For example, the mixing ratio of NH_3 would be $\sim 10^{-2}$ if all nitrogen is in NH_3 for the $100\times$ solar metallicity, and a reduction from that by three orders of magnitude would still result in a mixing ratio of 10^{-5}. Therefore, and as discussed in the main text, we do not expect the $100\times$ solar or higher metallicity massive atmosphere would likely become a false-positive imitation of small atmospheres.

Small atmosphere models. We use an atmospheric photochemical model[44] to simulate the atmospheric chemistry in small H_2 atmospheres and trace the steady-state abundances of CO, CH_4, C_2H_6, and other potential gases of interest. The photochemical model includes a comprehensive reaction network for O, H, C, N, and S species (including sulfur aerosols, hydrocarbons, and the reactions important in H_2 atmospheres), and it has been used to study the lifetime and equilibrium abundance of potential biosignature gases in H_2 atmospheres[61]. The pressure-temperature profiles (Fig. 5) used as the basis for the photochemical model are calculated with the climate module of 1D-TERRA[26]. The module uses a correlated-k approach with the random overlap method to include molecular absorption, collision-induced opacities, and the continuum of water vapor to calculate the radiative equilibrium, and the appropriate (moist or dry) adiabatic lapse rate to apply the convection adjustment. The module has been tested against the cases of Earth, Venus, and Mars, as well as with other radiative-convective and 3D climate models for modeling steam atmospheres[26].

As examples, we study H_2 atmospheres of 1 bar on a sub-Neptune planet that has a stellar irradiance similar to Earth and orbits around an early M star similar to K2-18. A 1-bar H_2 atmosphere on such a planet would likely have a surface temperature consistent with a liquid-water ocean (Fig. 5). For this planet, a 10-bar endowment of H_2 would result in a massive steam atmosphere, making it uninhabitable[26]. We adopt the "water-world" interpretation of the $1.7-3.5\ R_\oplus$ planet population that centers at $10\ M_\oplus$, and $2.5\ R_\oplus$[15,21], and assume 50% of water by mass in this study. In this interpretation, many sub-Neptunes may be ocean planets with deep oceans that do not require a massive H_2 envelope to explain their radius, and can conceivably have moderate-size H_2 atmospheres. This may not be directly applicable for K2-18 b, which resides on the low-density side of the $1.7-3.5\ R_\oplus$ population. The specific choices of these parameters are however unimportant, because atmospheric chemistry is not sensitive to moderate changes in the surface gravity.

The mixing ratio of N_2 on such a planet is probably set by atmospheric evolution (as opposed to the solubility equilibrium or geological recycling) and is assumed here to be 1%. As N_2 only minimally participates in the chemical cycles and does not have strong spectral features in the infrared, its exact abundance is not our main

concern. The photochemical model indicates that the NH_3 produced by photodissociation of N_2 in H_2 atmospheres has negligible mixing ratios ($< 10^{-12}$, see below).

CO_2 is the main form of carbon in thermochemical equilibrium with H_2O[32,38]. If a liquid-water ocean exists, the partial pressure of CO_2 is set by atmosphere-ocean partitioning, which in turn is mainly controlled by the oceanic pH[39–42]. The pH is affected by the abundance of cations in the ocean, which come from complex water-rock reactions and dissolution of the seafloor. The rates of the processes involved are uncertain; therefore, we explore the mixing ratio of CO_2 from 400 ppm to 10%, corresponding to the pCO_2 range from the present-day Earth to early Earth[62] and including the predicted range for ocean planets[41] that is still consistent with an H_2-dominated atmosphere.

Is the 400-ppm CO_2, or 4×10^{-4} bar partial pressure in a 1-bar atmosphere, a reasonable lower bound of the CO_2 partial pressure on a water world? We consider this question from a cosmochemical and geochemical perspective. Assuming equilibrium (during planet formation) between a Fe-core, a silicate mantle, and a well-mixed supercritical volatile envelope, the partitioning of C mass between reservoirs is described by

$$\mathrm{C_{total}} = \mathrm{C_{core}} + \mathrm{C_{silicate}} + \mathrm{C_{envelope}}, \tag{1}$$

where all reservoir masses are in kg, and

$$\mathrm{C_{core}}/\mathrm{M_{core}} = \mathrm{D_C}(\mathrm{C_{silicate}}/\mathrm{M_{silicate}}), \tag{2}$$

where $\mathrm{D_C}$ is a dimensionless partition coefficient, $\mathrm{M_{core}}$ (kg) is the mass of the Fe-dominated core, and $\mathrm{M_{silicate}}$ (kg) is the mass of the silicate mantle (molten during planet formation). For the partitioning between the envelope and the silicate mantle,

$$\mathrm{C_{envelope}k}(\mathrm{g_{esi}}/\mathrm{A_{esi}})(\mu_{\mathrm{avg}}/\mu_{\mathrm{C}})\mathrm{s_C} = \mathrm{C_{silicate}}/\mathrm{M_{silicate}}, \tag{3}$$

where k is a stochiometric correction from C mass to the mass of the C-bearing species in the envelope (i.e., $44/12 \sim 3.7$ for CO_2), $\mathrm{g_{esi}}$ is gravitational acceleration at the envelope-silicate interface in m s^{-2}, $\mathrm{A_{esi}}$ is the area of the envelope-silicate interface in m^2, μ_{avg} is the average molecular weight of the envelope (in Da), μ_{C} is the

molecular weight of the C-bearing species (in Da), and s_C is the solubility of the C-bearing species (in Pa^{-1}). Here we have assumed that the molten silicate layer is well-stirred.

Supposing $M_{core}/M_{silicate} \sim 0.5$ (like Earth) and $D_C \sim 10^3$ [63], then $C_{core}/C_{silicate} \sim 500$. If $C_{silicate}/M_{silicate} \sim 50$ ppm then $C_{core}/M_{core} \sim 2.5$ wt%, or $C_{total}/(M_{core} + M_{silicate}) \sim 1$ wt%, which is a reasonable lower bound for the primordial carbon endowment (see below). For $s_C = 0.55$ ppm/Mpa[64], the envelope partial pressure of the C species ($= C_{envelope} k (g_{esi}/A_{esi})(\mu_{avg}/\mu_C)$) is $\sim 10^3$ bars. For a $5 - M_\oplus$ and $1.5 - R_\oplus$ core+mantle[15] that defines the envelope-silicate boundary, and $\mu_{avg}/\mu_C = 0.4$ (appropriate for CO_2 in a H_2O-dominated supercritical layer during planet formation), the CO_2 mass in the envelope is 0.2% of an Earth mass. This estimate shows that even though most C is in the core, still-significant reservoirs of C exist both in the silicate and in the envelope[64–67]. Recent indications that the partition coefficient D_C is $\ll 10^3$ at the pressures and temperatures that are relevant for assembly of sub-Neptunes[68] would imply even more envelope C enrichment.

Following the formation of the liquid-water ocean, almost all of the CO_2 will be dissolved in the ocean. For a $5 - M_\oplus$ water layer, the CO_2 mass in the envelope estimated above corresponds to a concentration of ~ 0.01 mol/L of dissolved CO_2. Here we have also assumed that the ocean is well-stirred. A higher oceanic pH leads to more effective dissolution and less CO_2 in the atmosphere. As an extreme, if cations are leached from the silicate and not charge-balanced by chloride ions, then an ocean composition with a pH of 9 – 10 ("a soda lake") will result[69]. Using the equilibrium constant of carbonate and bicarbonate dissociation[70], the CO_2 partial pressure in equilibrium with this ocean would be $5 \times 10^{-5} \sim 7 \times 10^{-4}$ bar, which is consistent with the assumed lower bound.

The partition coefficient gives the ratios of concentration of a species in the Fe-dominated core to the concentration of the same species in the silicate mantle. Therefore doubling the total amount of C in the core+mantle will double the concentration in the magma. What is the whole-planet C content? In principle, a planet can form without accreting volatiles. However, a thin-atmosphere sub-Neptune must have a thick volatile (H_2O) layer in order to match density data. It is very likely that a world that forms with 10s of wt% H_2O will also accrete abundant C. We develop this point in more detail in the following paragraph.

At $T_{\rm eff} \sim 300$ K, the minimum liquid water content to explain most sub-Neptune masses and radii is $>\sim 50$ wt% even if there is no Fe-metal core[16]. This is more H_2O than can possibly be produced by hydrogen-magma reactions[71], and instead implies a contribution of planet building blocks from the temperature range beyond the water ice snowline. This is a zone where (in the Solar System), abundant refractory carbon is found. Specifically, the carbon content of primitive chondrite meteorites (CI and CM type) is 2-6 wt%[72]. Although we do not fully understand the origin of this refractory carbon, proposed mechanisms for forming this refractory carbon would also apply to exoplanetary systems[73]. Therefore we assume a planet bulk composition of $(2 - 6\ \mathrm{wt}\%) \times (1 - \mathrm{x})$ carbon, where x is the H_2O mass fraction, and the remainder of the planet's building blocks are assumed to have a C content similar to that of primitive chondrites. This is a conservative lower limit on bulk C content for a thin-H_2-atmosphere sub-Neptune, for the following two reasons. (i) It considers only refractory C, not C ices (e.g., CO_2 ice) which could be important in the case of whole-planet migration. (ii) Some primitive bodies in the Solar System appear to be more C-rich than the most primitive chondrite meteorites; for example, the surface of the dwarf planet Ceres may contain 20 wt% C[74]. These large bulk C contents map to substantial envelope C contents (Equations 1-3). As such, the 4×10^{-4} bar partial pressure of CO_2, while not the absolute lower limit, is a cosmochemically and geologically reasonable lower bound of the CO_2 partial pressure on a water world.

The pressure at the water-rock boundary of a $10 - M_\oplus$ and $2.5 - R_\oplus$ planet is ~ 500 GPa[75,76], and this overloading pressure should suppress volcanism completely[41,77,78]. Therefore we do not include any volcanic outgassing in the standard models. As variant models, we consider the possibility of minor and intermittent sources of CO into the atmosphere. Evaporation of meteorites may provide a source of CO and CO_2[79], and water-rock reactions at the temperature relevant to the "fuzzy layer" may produce CO (and not CH_4 as it is thermochemically disfavored at high temperatures). The rates of these processes are unknown, but numerical experiments with the photochemical model indicate that an additional CO source of 10^{10} molecule cm^{-2} s^{-1} would lead to a steady-state abundance of CO greater than that of H_2, effectively resulting in a CO-dominated atmosphere. A CO source of 10^9 molecule cm^{-2} s^{-1} would produce the CO-dominated atmosphere in the 10%-CO_2 case but not in the 400ppm-CO_2 case. We therefore include a low-CO_2 case with the CO source of 10^9

molecule cm^{-2} s^{-1} as a variant model.

Table 1 summarizes the input parameters and results of the photochemical models, and Fig. 6 shows the vertical profiles of main gases and photochemical products. CO is produced from the photodissociation of CO_2 and can build up to the 10^{-5} and 10^{-2} mixing ratio level for the low-CO_2 and the high-CO_2 cases. OH from the photodissociation of H_2O destroys CO and maintains its steady-state mixing ratio. CH_4 is also produced photochemically and can build up to a substantial mixing ratio ($\sim 10^{-3}$) in the low-CO_2 case. The abundance of CH_4 is much smaller in the high-CO_2 case, because of a more oxidized atmosphere. Together with the high CH_4 mixing ratio, C_2H_6 is produced in the low-CO_2 case and can accumulate to a mixing ratio of $\sim 10^{-7}$. C_2H_2, as expected, is short-lived and only has significant mixing ratios in the upper atmosphere. Here we have applied a deposition velocity of 10^{-5} cm s^{-1} to account for the loss of carbon due to organic haze formation and deposition[44]; removing this sink does not substantially change the results shown in Fig. 6. The additional source of CO would result in moderately more CO, CH_4, and C_2H_6 in the atmosphere (Model 1a in Table 1 and Fig. 6). We see that CO, and in the low-CO2 case, CH_4, can build up to the mixing ratio levels that cause significant features in the planet's transmission spectrum (Fig. 3).

Before closing this section, we address whether NH_3 can be produced substantially by water-rock reactions and then emitted into the atmosphere. Hydrothermal systems on early Earth may produce NH_3 from the reduction of nitrite and nitrate[80,81]. On a planet with an H_2-dominated atmosphere, however, atmospheric production of the oxidized nitrogen including nitrite and nitrate should be very limited. Moreover, the storage capability of NH_3 by the ocean is vast and limits the emission into the atmosphere. At the pH value of 8 (a lower pH would further favor the partitioning of NH_3 in the ocean), 10^{-6} bar of atmospheric NH_3 requires a dissolved ammonium concentration of 10^{-3} mol/L in equilibrium[70]. The mass of NH_3 in the atmosphere and ocean is then $\sim 10^{-5}$ of the planetary mass. This would only be possible if much of the planet's rocky core begins with a volatile composition similar to carbonaceous chondrites, and most of this nitrogen is partitioned into the atmosphere and ocean as NH_3[82], which is highly unlikely as N_2 is thermochemically favored. Therefore, the concentration of dissolved NH_3 should be

small and so is the atmospheric NH_3 on a planet with a massive ocean.

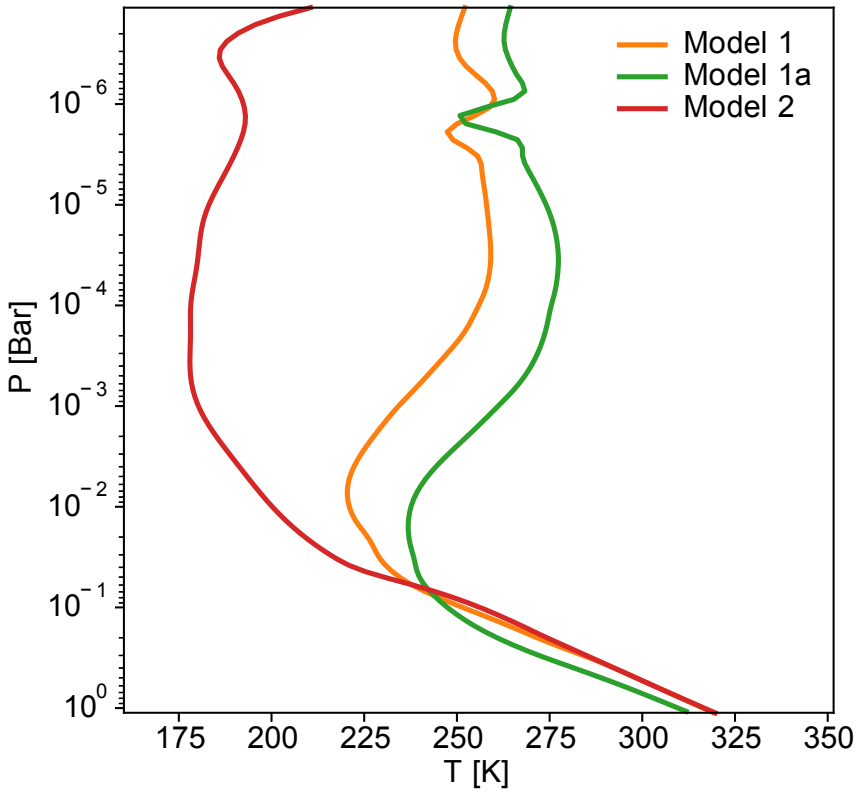

Figure 5: Modeled pressure-temperature profiles in a cold sub-Neptune like K2-18 b that has a small H_2 atmosphere. For the stellar irradiance, we use $S = S_{\rm Earth} * (1 - A_{\rm B})$, with a Bond albedo of $A_{\rm B} = 0.3$ (similar to Earth), to account for the radiative effects clouds would have in the otherwise cloud-free climate model. The surface albedo reflects a dark ocean (0.06) and convective adjustment follows a moist adiabat above the ocean. We show the results for the low-CO_2 case (Model 1 in Table 1), the low-CO_2 case with additional CO sources (Model 1a), and the high-CO_2 case (Model 2). The surface temperatures in these models are consistent with a liquid-water ocean.

1. Montet, B. T. *et al.* Stellar and planetary properties of k2 campaign 1 candidates and validation of 17 planets, including a planet receiving earth-like insolation. *The Astrophysical Journal* **809**, 25 (2015).

2. Gillon, M. *et al.* Seven temperate terrestrial planets around the nearby ultracool dwarf star trappist-1. *Nature* **542**, 456–460 (2017).

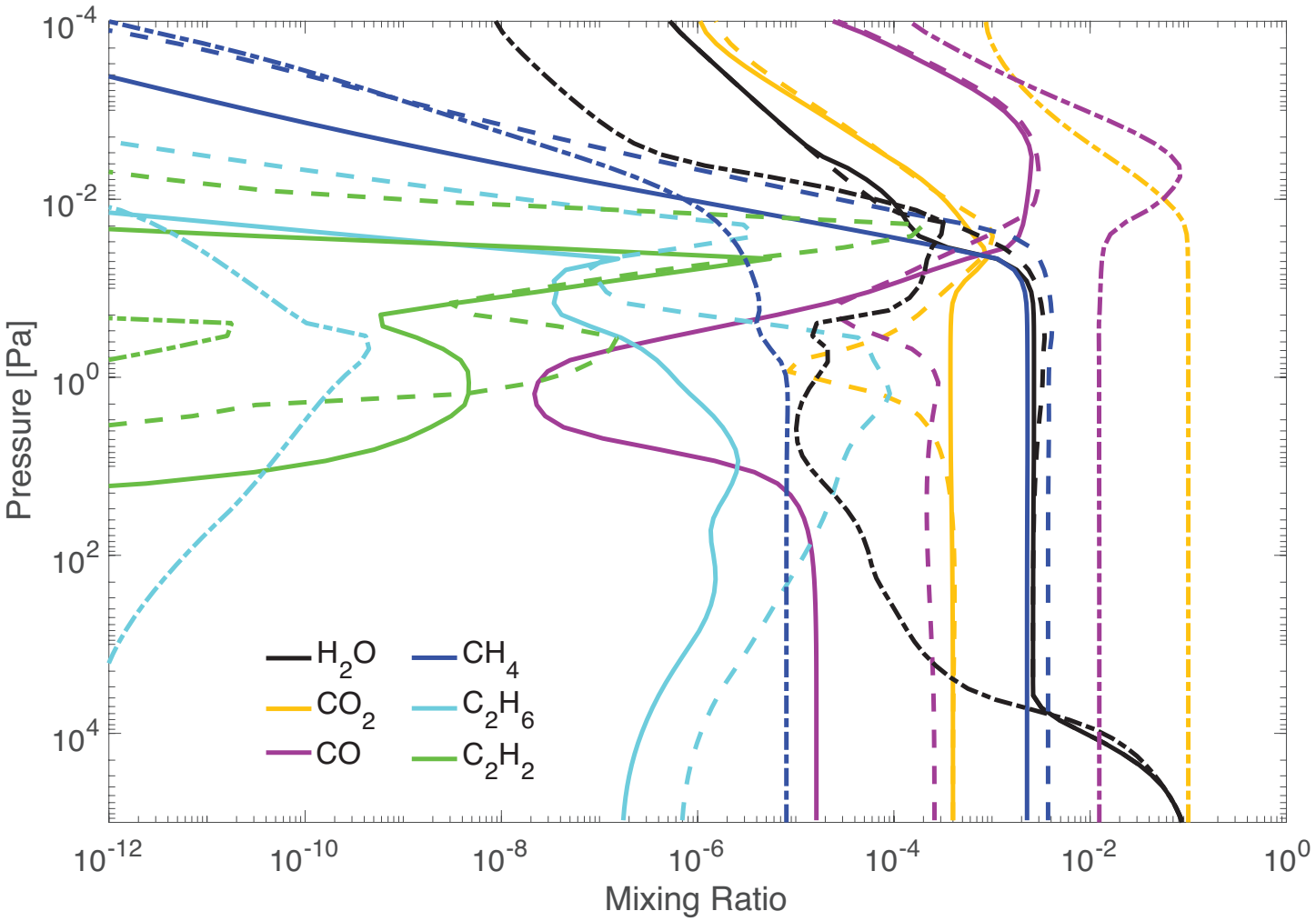

Figure 6: Modeled abundances of main gases and photochemical products in a cold sub-Neptune like K2-18 b that has a small H_2 atmosphere. Solid, dashed, and dash-dot lines show the results for the low-CO_2 case (Model 1 in Table 1), the low-CO_2 case with additional CO sources (Model 1a), and the high-CO_2 case (Model 2). The photochemical abundance of nitrogen molecules such as NH_3 and HCN is $< 10^{-12}$.

3. Dittmann, J. A. *et al.* A temperate rocky super-earth transiting a nearby cool star. *Nature* **544**, 333–336 (2017).

4. De Wit, J. *et al.* Atmospheric reconnaissance of the habitable-zone earth-sized planets orbiting trappist-1. *Nature Astronomy* **2**, 214–219 (2018).

5. Zhang, Z., Zhou, Y., Rackham, B. V. & Apai, D. The near-infrared transmission spectra of trappist-1 planets b, c, d, e, f, and g and stellar contamination in multi-epoch transit spectra. *The Astronomical Journal* **156**, 178 (2018).

6. Tsiaras, A., Waldmann, I. P., Tinetti, G., Tennyson, J. & Yurchenko, S. N. Water vapour in the atmosphere of the habitable-zone eight-earth-mass planet k2-18 b. *Nature Astronomy* **3**, 1086–1091 (2019).

7. Benneke, B. *et al.* Water vapor and clouds on the habitable-zone sub-neptune exoplanet k2-18b. *The Astrophysical Journal Letters* **887**, L14 (2019).

8. Pierrehumbert, R. & Gaidos, E. Hydrogen greenhouse planets beyond the habitable zone. *The Astrophysical Journal Letters* **734**, L13 (2011).

9. Ramirez, R. M. & Kaltenegger, L. A volcanic hydrogen habitable zone. *The Astrophysical Journal Letters* **837**, L4 (2017).

10. Koll, D. D. & Cronin, T. W. Hot hydrogen climates near the inner edge of the habitable zone. *The Astrophysical Journal* **881**, 120 (2019).

11. Madhusudhan, N., Nixon, M. C., Welbanks, L., Piette, A. A. & Booth, R. A. The interior and atmosphere of the habitable-zone exoplanet k2-18b. *The Astrophysical Journal Letters* **891**, L7 (2020).

12. Fulton, B. J. & Petigura, E. A. The california-kepler survey. vii. precise planet radii leveraging gaia dr2 reveal the stellar mass dependence of the planet radius gap. *The Astronomical Journal* **156**, 264 (2018).

13. Rogers, L. & Seager, S. Three possible origins for the gas layer on gj 1214b. *The Astrophysical Journal* **716**, 1208 (2010).

14. Valencia, D., Guillot, T., Parmentier, V. & Freedman, R. S. Bulk composition of gj 1214b and other sub-neptune exoplanets. *The Astrophysical Journal* **775**, 10 (2013).

15. Zeng, L. *et al.* Growth model interpretation of planet size distribution. *Proceedings of the National Academy of Sciences* **116**, 9723–9728 (2019).

16. Mousis, O. *et al.* Irradiated ocean planets bridge super-earth and sub-neptune populations. *The Astrophysical journal letters* **896**, L22 (2020).

17. Seager, S. *et al.* Absence of nh3 as a diagnostic for the presence of water oceans on temperate sub neptune-sized exoplanets. *AAS Journals* **Submitted** (2021).

18. Miller-Ricci, E., Seager, S. & Sasselov, D. The atmospheric signatures of super-earths: how to distinguish between hydrogen-rich and hydrogen-poor atmospheres. *The Astrophysical Journal* **690**, 1056 (2008).

19. Owen, J. E. & Wu, Y. The evaporation valley in the kepler planets. *The Astrophysical Journal* **847**, 29 (2017).

20. Jin, S. & Mordasini, C. Compositional imprints in density–distance–time: a rocky composition for close-in low-mass exoplanets from the location of the valley of evaporation. *The Astrophysical Journal* **853**, 163 (2018).

21. Venturini Corbellini, J. E., Guilera, O. M., Haldemann, J., Ronco, M. P. & Mordasini, C. The nature of the radius valley. *Astronomy and astrophysics* **643**, L1 (2020).

22. Robinson, T. D., Meadows, V. S. & Crisp, D. Detecting oceans on extrasolar planets using the glint effect. *The Astrophysical Journal Letters* **721**, L67 (2010).

23. Cowan, N. B. *et al.* Alien maps of an ocean-bearing world. *The Astrophysical Journal* **700**, 915 (2009).

24. Fan, S. *et al.* Earth as an exoplanet: A two-dimensional alien map. *The Astrophysical Journal Letters* **882**, L1 (2019).

25. Gaudi, B. S. *et al.* The Habitable Exoplanet Observatory (HabEx) Mission Concept Study Final Report. *arXiv e-prints* arXiv:2001.06683 (2020). 2001.06683.

26. Scheucher, M. *et al.* Consistently simulating a wide range of atmospheric scenarios for k2-18b with a flexible radiative transfer module. *The Astrophysical Journal* **898**, 44 (2020).

27. Lee, E. J. & Chiang, E. Breeding super-earths and birthing super-puffs in transitional disks. *The Astrophysical Journal* **817**, 90 (2016).

28. Loftus, K., Wordsworth, R. D. & Morley, C. V. Sulfate aerosol hazes and so2 gas as constraints on rocky exoplanets' surface liquid water. *The Astrophysical Journal* **887**, 231 (2019).

29. Blain, D., Charney, B. & B'ezard, B. 1d atmospheric study of the temperate sub-neptune k2-18b. *arXiv preprint arXiv:2011.10459* (2020).

30. Burrows, A. & Sharp, C. Chemical equilibrium abundances in brown dwarf and extrasolar giant planet atmospheres. *The Astrophysical Journal* **512**, 843 (1999).

31. Heng, K. & Tsai, S.-M. Analytical models of exoplanetary atmospheres. iii. gaseous c–h–o–n chemistry with nine molecules. *The Astrophysical Journal* **829**, 104 (2016).

32. Woitke, P. *et al.* Coexistence of ch4, co2 and h2o in exoplanet atmospheres. *arXiv preprint arXiv:2010.12241* (2020).

33. Morley, C. V. *et al.* Water clouds in y dwarfs and exoplanets. *The Astrophysical Journal* **787**, 78 (2014).

34. Charney, B., Blain, D., B'ezard, B., Leconte, J. & Turbet, M. Formation and dynamics of water clouds on temperate sub-neptunes: the example of k2-18b. *arXiv preprint arXiv:2011.11553* (2020).

35. Hu, R. Photochemical gases in cold and gaseous exoplanets and their spectral features. *The Astrophysical Journal* **submitted** (2021).

36. Hu, R., Seager, S. & Bains, W. Photochemistry in terrestrial exoplanet atmospheres. ii. h2s and so2 photochemistry in anoxic atmospheres. *The Astrophysical Journal* **769**, 6 (2013).

37. Zahnle, K., Marley, M. S., Morley, C. V. & Moses, J. I. Photolytic hazes in the atmosphere of 51 eri b. *The Astrophysical Journal* **824**, 137 (2016).

38. Hu, R. & Seager, S. Photochemistry in Terrestrial Exoplanet Atmospheres. III. Photochemistry and Thermochemistry in Thick Atmospheres on Super Earths and Mini Neptunes. **784**, 63 (2014). 1401.0948.

39. Kitzmann, D. *et al.* The unstable co2 feedback cycle on ocean planets. *Monthly Notices of the Royal Astronomical Society* **452**, 3752–3758 (2015).

40. Krissansen-Totton, J. & Catling, D. C. Constraining climate sensitivity and continental versus seafloor weathering using an inverse geological carbon cycle model. *Nature communications* **8**, 1–15 (2017).

41. Kite, E. S. & Ford, E. B. Habitability of exoplanet waterworlds. *The Astrophysical Journal* **864**, 75 (2018).

42. Isson, T. T. & Planavsky, N. J. Reverse weathering as a long-term stabilizer of marine ph and planetary climate. *Nature* **560**, 471–475 (2018).

43. Vazan, A., Sari, R. & Kessel, R. A new perspective on interiors of ice-rich planets: Ice-rock mixture rather than a layered structure. *arXiv preprint arXiv:2011.00602* (2020).

44. Hu, R., Seager, S. & Bains, W. Photochemistry in terrestrial exoplanet atmospheres. i. photochemistry model and benchmark cases. *The Astrophysical Journal* **761**, 166 (2012).

45. Cloutier, R. *et al.* Confirmation of the radial velocity super-earth k2-18c with harps and carmenes. *Astronomy & Astrophysics* **621**, A49 (2019).

46. France, K. *et al.* The muscles treasury survey. i. motivation and overview. *The Astrophysical Journal* **820**, 89 (2016).

47. dos Santos, L. A. *et al.* The high-energy environment and atmospheric escape of the mini-neptune k2-18 b. *Astronomy & Astrophysics* **634**, L4 (2020).

48. Batalha, N. E. *et al.* Pandexo: a community tool for transiting exoplanet science with jwst & hst. *Publications of the Astronomical Society of the Pacific* **129**, 064501 (2017).

49. Waldmann, I. P. *et al.* Tau-rex i: A next generation retrieval code for exoplanetary atmospheres. *The Astrophysical Journal* **802**, 107 (2015).

50. Changeat, Q. *et al.* Disentangling atmospheric compositions of k2-18 b with next generation facilities. *arXiv preprint arXiv:2003.01486* (2020).

51. Belu, A. *et al.* Primary and secondary eclipse spectroscopy with jwst: exploring the exoplanet parameter space. *Astronomy & Astrophysics* **525**, A83 (2011).

52. Krissansen-Totton, J., Garland, R., Irwin, P. & Catling, D. C. Detectability of biosignatures in anoxic atmospheres with the james webb space telescope: A trappist-1e case study. *The Astronomical Journal* **156**, 114 (2018).

53. Wunderlich, F. *et al.* Detectability of atmospheric features of earth-like planets in the habitable zone around m dwarfs. *Astronomy & Astrophysics* **624**, A49 (2019).

54. Pidhorodetska, D., Fauchez, T. J., Villanueva, G. L., Domagal-Goldman, S. D. & Kopparapu, R. K. Detectability of molecular signatures on trappist-1e through transmission spectroscopy simulated for future space-based observatories. *The Astrophysical Journal Letters* **898**, L33 (2020).

55. Gialluca, M., Robinson, T., Rugheimer, S. & Wunderlich, F. Characterizing atmospheres of transiting earth-like exoplanets orbiting m dwarfs with james webb space telescope. *arXiv preprint arXiv:2101.04139* (2021).

56. Fortney, J. J. *et al.* Beyond equilibrium temperature: How the atmosphere/interior connection affects the onset of methane, ammonia, and clouds in warm transiting giant planets. *The Astronomical Journal* **160**, 288 (2020).

57. Zahnle, K. J. & Marley, M. S. Methane, carbon monoxide, and ammonia in brown dwarfs and self-luminous giant planets. *The Astrophysical Journal* **797**, 41 (2014).

58. Tsai, S.-M. *et al.* Toward consistent modeling of atmospheric chemistry and dynamics in exoplanets: Validation and generalization of the chemical relaxation method. *The Astrophysical Journal* **862**, 31 (2018).

59. Visscher, C., Moses, J. I. & Saslow, S. A. The deep water abundance on jupiter: New constraints from thermochemical kinetics and diffusion modeling. *Icarus* **209**, 602–615 (2010).

60. Visscher, C. & Moses, J. I. Quenching of carbon monoxide and methane in the atmospheres of cool brown dwarfs and hot jupiters. *The Astrophysical Journal* **738**, 72 (2011).

61. Seager, S., Bains, W. & Hu, R. Biosignature gases in h2-dominated atmospheres on rocky exoplanets. *The Astrophysical Journal* **777**, 95 (2013).

62. Catling, D. C. & Kasting, J. F. *Atmospheric evolution on inhabited and lifeless worlds* (Cambridge University Press, 2017).

63. Dasgupta, R. Ingassing, storage, and outgassing of terrestrial carbon through geologic time. *Reviews in Mineralogy and Geochemistry* **75**, 183–229 (2013).

64. Dasgupta, R. & Grewal, D. S. Origin and early differentiation of carbon and associated life-essential volatile elements on earth. *Deep Carbon* 4–39 (2019).

65. Bergin, E. A., Blake, G. A., Ciesla, F., Hirschmann, M. M. & Li, J. Tracing the ingredients for a habitable earth from interstellar space through planet formation. *Proceedings of the National Academy of Sciences* **112**, 8965–8970 (2015).

66. Keppler, H. & Golabek, G. Graphite floatation on a magma ocean and the fate of carbon during core formation. *Geochem. Perspect. Lett.* **11**, 12–17 (2019).

67. Hirschmann, M. M. Constraints on the early delivery and fractionation of earth's major volatiles from c/h, c/n, and c/s ratios. *American Mineralogist* **101**, 540–553 (2016).

68. Fischer, R. A., Cottrell, E., Hauri, E., Lee, K. K. & Le Voyer, M. The carbon content of earth and its core. *Proceedings of the National Academy of Sciences* **117**, 8743–8749 (2020).

69. Kempe, S. & Degens, E. T. An early soda ocean? *Chemical Geology* **53**, 95–108 (1985).

70. Seinfeld, J. H. & Pandis, S. N. *Atmospheric chemistry and physics: from air pollution to climate change* (John Wiley & Sons, 2016).

71. Kite, E. S. & Schaefer, L. Water on hot rocky exoplanets. *The Astrophysical Journal Letters* **909**, L22 (2021).

72. Pearson, V., Sephton, M., Franchi, I., Gibson, J. & Gilmour, I. Carbon and nitrogen in carbonaceous chondrites: Elemental abundances and stable isotopic compositions. *Meteoritics & Planetary Science* **41**, 1899–1918 (2006).

73. Bergin, E., Cleeves, L. I., Crockett, N. & Blake, G. Exploring the origins of carbon in terrestrial worlds. *Faraday discussions* **168**, 61–79 (2014).

74. Marchi, S. *et al.* An aqueously altered carbon-rich ceres. *Nature Astronomy* **3**, 140–145 (2019).

75. Sotin, C., Grasset, O. & Mocquet, A. Mass–radius curve for extrasolar earth-like planets and ocean planets. *Icarus* **191**, 337–351 (2007).

76. Levi, A., Sasselov, D. & Podolak, M. Structure and dynamics of cold water super-earths: the case of occluded ch4 and its outgassing. *The Astrophysical Journal* **792**, 125 (2014).

77. Kite, E. S., Manga, M. & Gaidos, E. Geodynamics and rate of volcanism on massive earth-like planets. *The Astrophysical Journal* **700**, 1732 (2009).

78. Noack, L., Rivoldini, A. & Van Hoolst, T. Volcanism and outgassing of stagnant-lid planets: Implications for the habitable zone. *Physics of the Earth and Planetary Interiors* **269**, 40–57 (2017).

79. Schaefer, L. & Fegley Jr, B. Redox states of initial atmospheres outgassed on rocky planets and planetesimals. *The Astrophysical Journal* **843**, 120 (2017).

80. Summers, D. P. & Chang, S. Prebiotic ammonia from reduction of nitrite by iron (ii) on the early earth. *Nature* **365**, 630–633 (1993).

81. Summers, D. P. Ammonia formation by the reduction of nitrite/nitrate by fes: ammonia formation under acidic conditions. *Origins of Life and Evolution of Biospheres* **35**, 299–312 (2005).

82. Marty, B. *et al.* Origins of volatile elements (h, c, n, noble gases) on earth and mars in light of recent results from the rosetta cometary mission. *Earth and Planetary Science Letters* **441**, 91–102 (2016).

Acknowledgements The authors thank helpful discussions with Fabrice Gaillard and Sukrit Ranjan. This work was supported in part by NASA Exoplanets Research Program grant #80NM0018F0612. The research was carried out at the Jet Propulsion Laboratory, California Institute of Technology, under a contract with the National Aeronautics and Space Administration.

Author Contribution RH conceived and designed the study, simulated the photochemical models, interpreted the results, and wrote the manuscript. MD performed the JWST observation simulations and atmospheric retrievals. MS computed the pressure-temperature profiles. EK derived the cosmochemical and geological lower bounds for the carbon content. SS contributed interior structure models and insights. HR oversaw the development of the radiative-convective model used in the study. All authors commented on the overall narrative of the paper.

Competing Interests The authors declare that they have no competing financial interests.

Correspondence Correspondence and requests for materials should be addressed to Renyu Hu (email: renyu.hu@jpl.nasa.gov).

Data Availability The raw data that are used to generate the figures in this paper are available from the corresponding author upon reasonable request.

Code Availability The photochemical code used in this study is written in C and will be released for unlimited re-use at GitHub. The radiative-convective model used in the study is proprietary to Deutsches Zentrum für Luft- und Raumfahrt and requests for collaboration should be addressed to Heike Rauer (Heike.Rauer@dlr.de).

Supplementary Information Supplementary Information is available for this paper.

1 Supplementary Information A: XXX

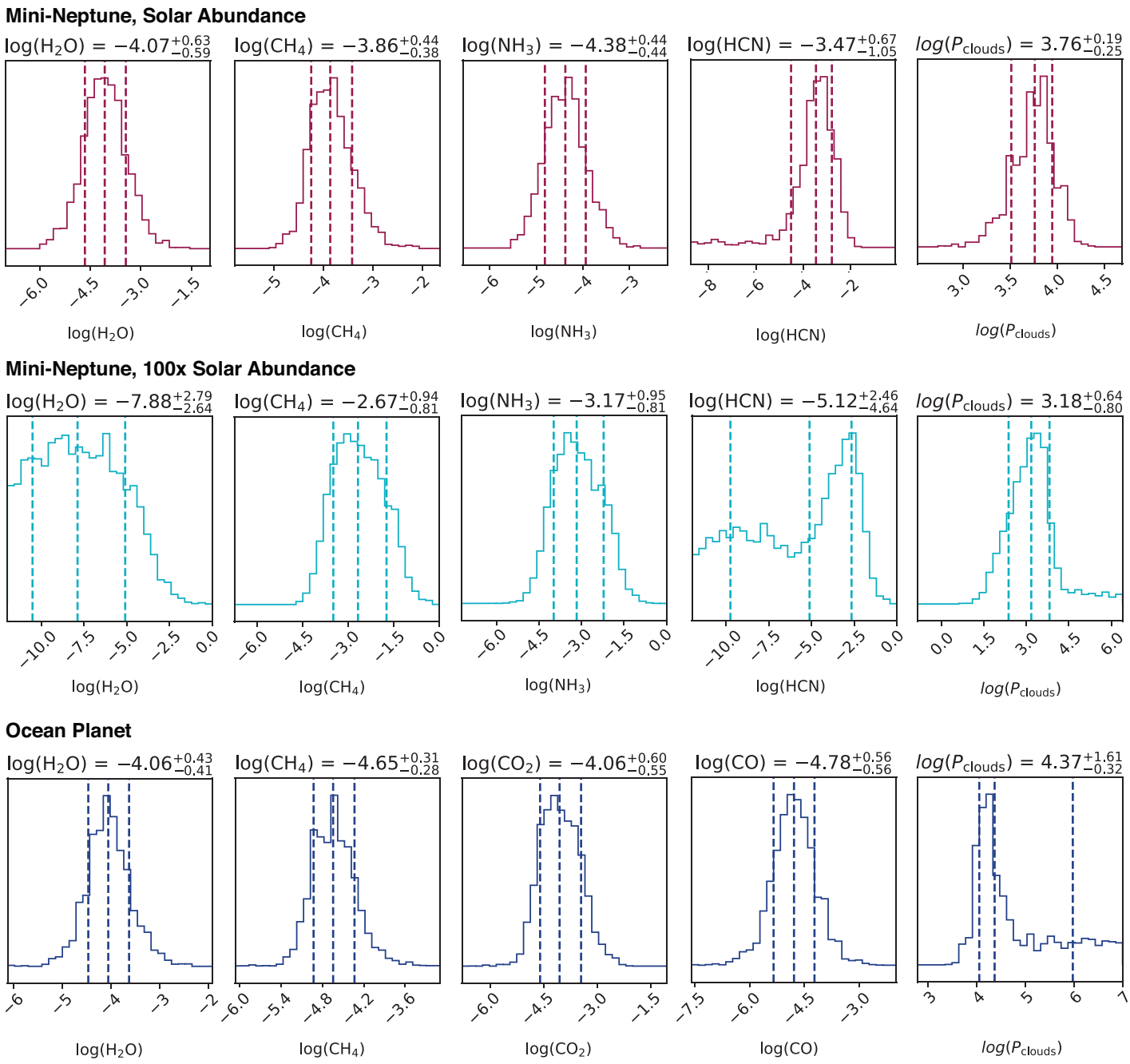

Figure S1: Retrieved posterior distributions of the abundances of the main chemical compounds and the cloud pressure in example massive-atmosphere and small-atmosphere scenarios. The input transmission spectra are shown in Fig. 3 and the expected uncertainties are calculated using PandExo[48], assuming to observe two transits of K2-18 b with NIRSpec/G235H and four transits with NIRSpec/G395H. A detailed characterization of the atmosphere of K2-18 b, including distinguishing a small atmosphere versus a massive one and measuring the abundances of H_2O, CH_4, NH_3, HCN, CO_2, and CO, will be achievable with moderate time investment of JWST.

Model	Name	CO_2	CO flux	CO	CH_4	C_2H_6
			cm^{-2} s^{-1}			
1	Low-CO_2	4×10^{-4}	0	1.6×10^{-5}	2.3×10^{-3}	2.2×10^{-7}
1a	Low-CO_2 Variant	4×10^{-4}	1.0×10^{9}	2.6×10^{-4}	3.7×10^{-3}	9.0×10^{-7}
2	High-CO_2	0.1	0	1.2×10^{-2}	8.0×10^{-6}	$< 10^{-12}$

Table 1: Summary of the photochemical model parameters and results. The volume mixing ratios of CO_2 (as inputs), CO, CH_4, and C_2H_6 (as results) are column-averaged and dimensionless.

Figures

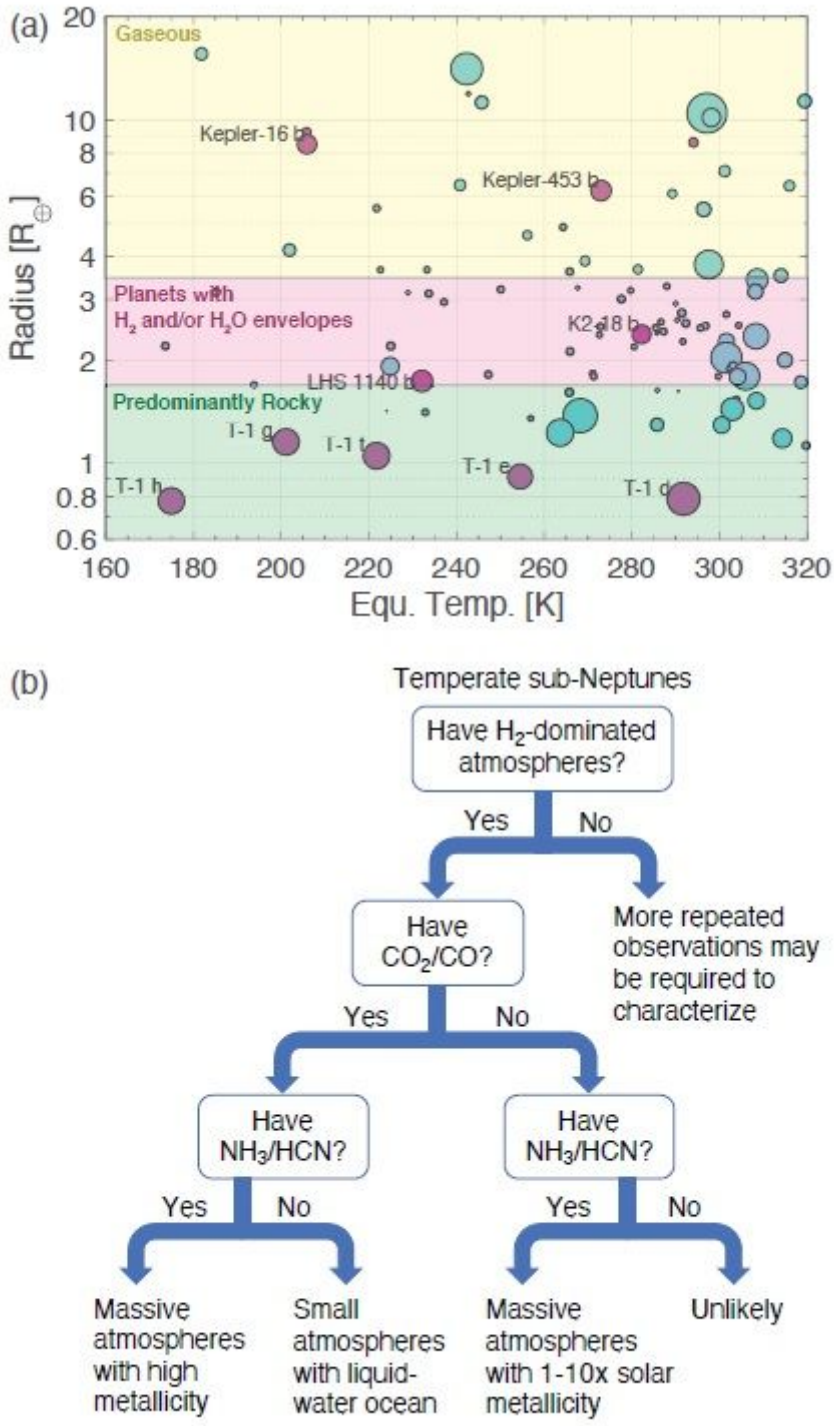

Figure 1

Temperate exoplanets amenable for atmospheric characterization via transmission spectroscopy. (a) Purple dots are confirmed planets with measured masses, and blue dots are planets with unknown masses or planet candidates. Data are taken from the NASA Exoplanet Archive and and the TESS Objects

of Interest Catalog. The marker sizes are scaled with the expected S/N of the spectral features of an H2 atmosphere observed by JWST at 2 μm. Most of the temperate planets and planet candidates suitable for atmospheric characterization are larger than Earth and thus more likely to have H2 atmospheres. (b) A roadmap to characterize the mass of the atmospheres and the habitability of temperate sub-Neptunes by detecting signature gases. See text for details.

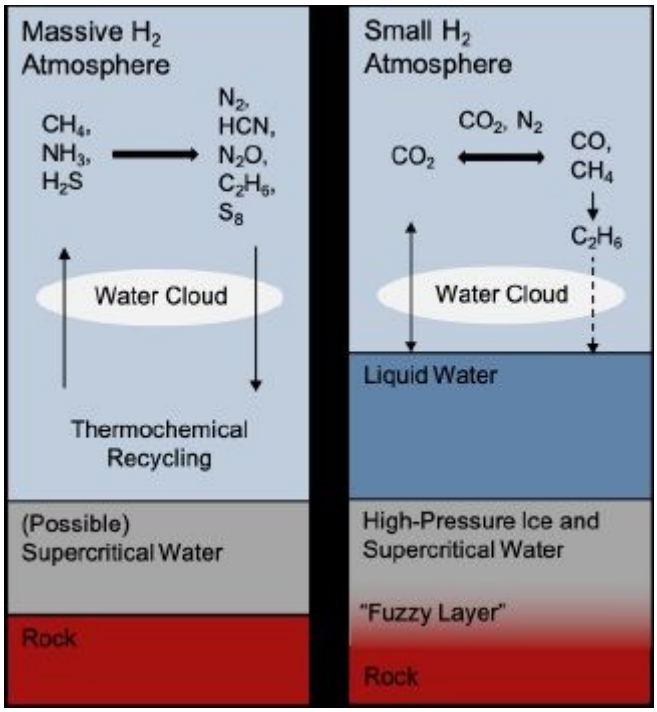

Figure 2

Interior structures of temperate H-rich exoplanets and the associated ranges of atmospheric composition. If the planet has a massive H2 atmosphere, the deep atmosphere would be hot – enabling thermochemical recycling – but a liquid-water surface would not be possible. If the planet has a small H2 atmosphere, a liquid-water surface may be possible. On these planets, the equilibrium abundance of atmospheric CO2 is set by the oceanic chemistry and that of N2 by atmospheric evolution.

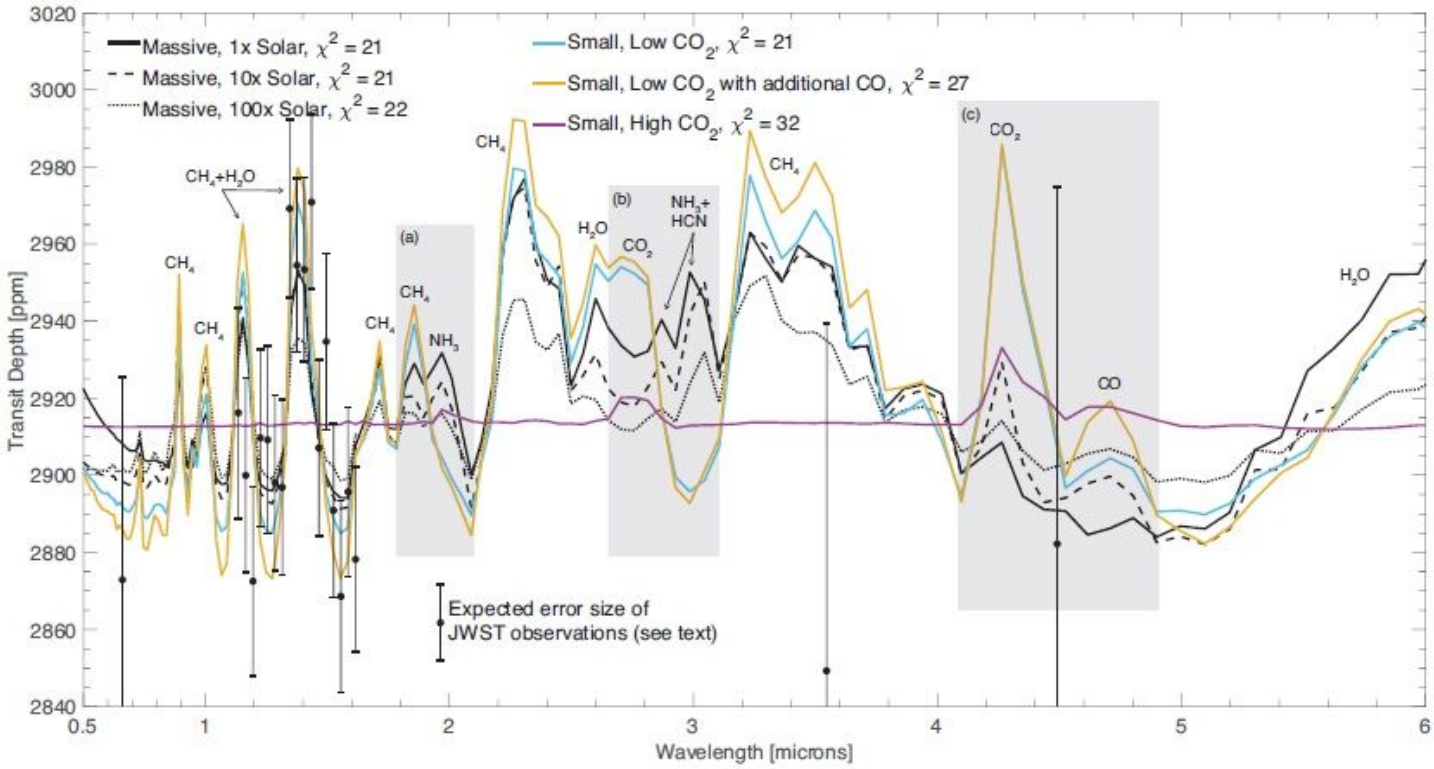

Figure 3

Expected transmission spectrum of temperate sub-Neptune planets of M dwarf stars, using K2-18 b as an example and comparing with the planet's transit depth observed by K2, Hubble and Spitzer7. The massive-H2-atmosphere models and the small-H2-atmosphere models differ in three spectral regions: in (a) and (b), the massive-atmosphere models have absorption features of NH3 and HCN, while the small-atmosphere models do not; in (c), the small-atmosphere models with a low mixing ratio of CO2 (400 ppm) have prominent features of CO2 and CO, while the massive-atmosphere models only have small features of CO2. The small-atmosphere models with a high mixing ratio of CO2 (10%) has a high mean molecular weight (7) and a cloud top at 10−3 bar (as opposed to 3 × 10−2 bar the low-CO2 cases) and thus muted spectral features.

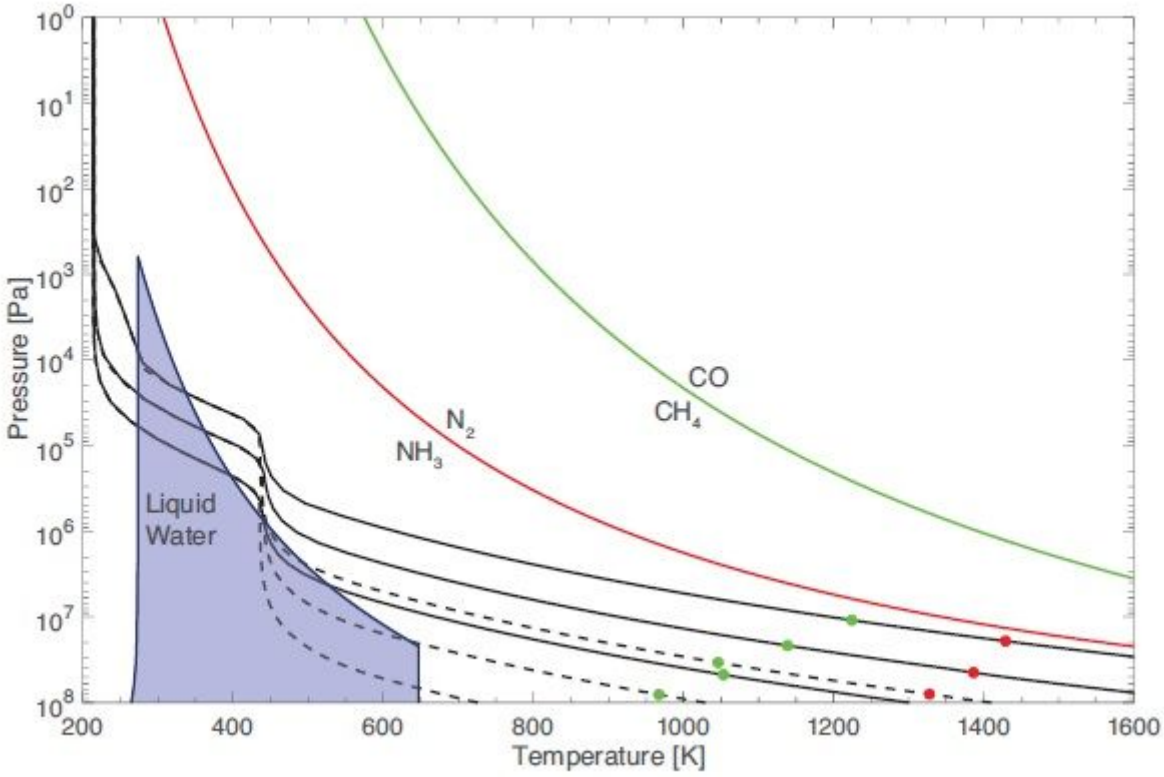

Figure 4

Modeled pressure-temperature profiles of a sub-Neptune exoplanet like K2-18 b with massive H2 atmospheres that receive stellar irradiance of Earth's, for an internal heat flux of Tint = 60 K (similar to Neptune, black solid lines) and Tint = 30 K (similar to Earth, black dashed lines). The pressure-temperature profiles assume 1×, 10×, and 100× solar metallicity. The shaded area shows the pressure and temperature range where pure liquid water is stable. The green and red lines show the equal-abundance boundaries for major carbon and nitrogen gases in a solar-metallicity gas in thermochemical equilibrium, and the green and red dots show the expected quench point for CO and that for N2 respectively. The quench points are estimated by equating the chemical lifetime to the vertical mixing timescale57, 58, 60, with the eddy diffusion coefficient estimated using a mixing-length theory59 (104 m2 s−1 at the pressure of 106 – 108 Pa). The quench point for CO2 follows that of CO, and similarly, that of HCN occurs at a similar pressure and temperature as N257, 58.

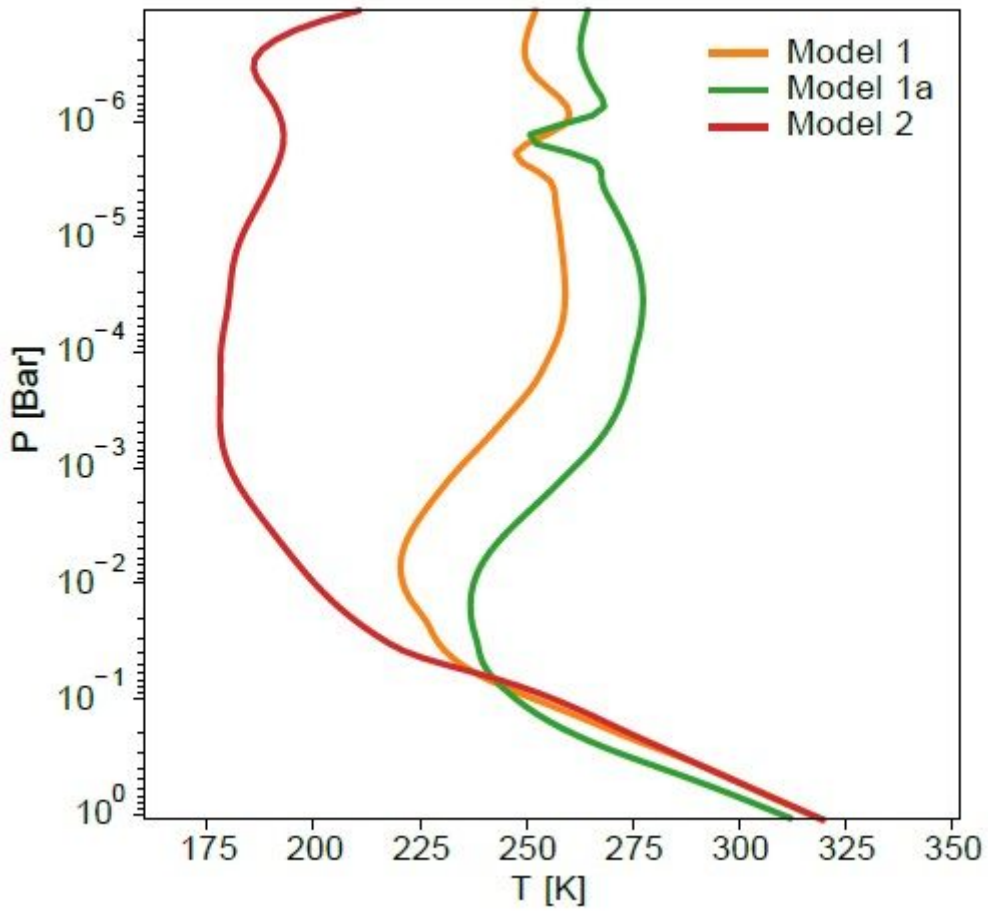

Figure 5

Modeled pressure-temperature profiles in a cold sub-Neptune like K2-18 b that has a small H2 atmosphere. For the stellar irradiance, we use S = SEarth □ (1 − AB), with a Bond albedo of AB = 0.3 (similar to Earth), to account for the radiative effects clouds would have in the otherwise cloud-free climate model. The surface albedo reflects a dark ocean (0.06) and convective adjustment follows a moist adiabat above the ocean. We show the results for the low-CO2 case (Model 1 in Table 1), the low-CO2 case with additional CO sources (Model 1a), and the high-CO2 case (Model 2). The surface temperatures in these models are consistent with a liquid-water ocean.

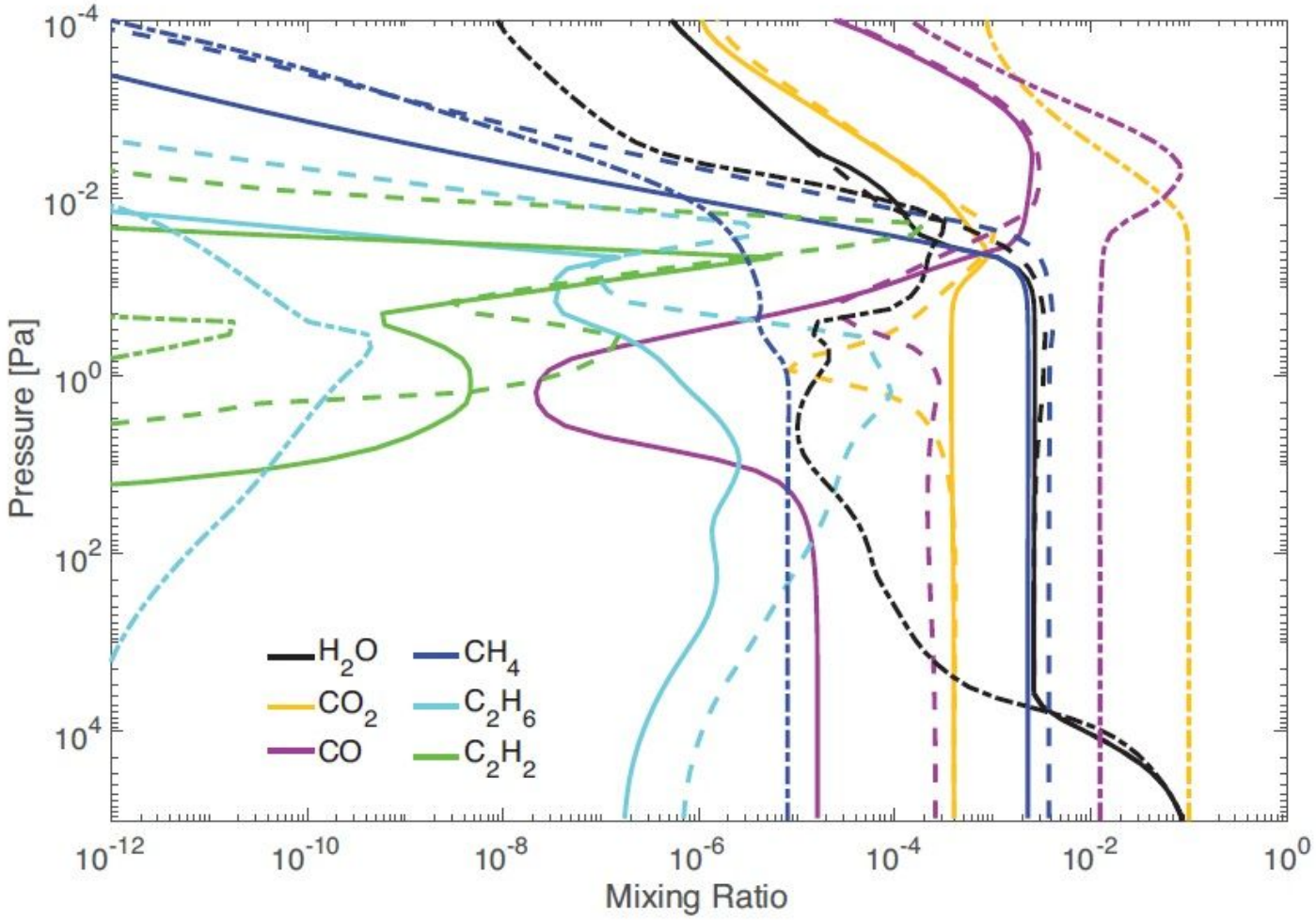

Figure 6

Modeled abundances of main gases and photochemical products in a cold sub-Neptune like K2-18 b that has a small H2 atmosphere. Solid, dashed, and dash-dot lines show the results for the low-CO2 case (Model 1 in Table 1), the low-CO2 case with additional CO sources (Model 1a), and the high-CO2 case (Model 2). The photochemical abundance of nitrogen molecules such as NH3 and HCN is < 10−12.